IJIRSET
International Journal of Innovative Research in
SCIENCE | ENGINEERING | TECHNOLOGY

e-ISSN: 2319-8753 | p-ISSN: 2347-6710

INTERNATIONAL JOURNAL OF INNOVATIVE RESEARCH

IN SCIENCE | ENGINEERING | TECHNOLOGY

Volume 12, Issue 7, July 2023

INTERNATIONAL STANDARD SERIAL NUMBER INDIA

Impact Factor: 8.423

9940 572 462 | 6381 907 438 | ijirset@gmail.com | www.ijirset.com

International Journal of Innovative Research in Science, Engineering and Technology (IJIRSET)

|e-ISSN: 2319-8753, p-ISSN: 2347-6710| www.ijirset.com | Impact Factor: 8.423| A Monthly Peer Reviewed & Referred Journal |

|| Volume 12, Issue 7, July 2023 ||

| DOI:10.15680/IJIRSET.2023.1207220 |

Reliability Degradation Mechanisms in Smart Wire Photovoltaic Modules

Sekhar Tatineni

Senior Director, Engineering & Production Systems Development, Singapore

ABSTRACT: Smart Wire Connection Technology modules have now accumulated between two and six years of field operational service at scale across geographically and climatically diverse installations, enabling a rigorous assessment of reliability performance under real deployment conditions. This report presents a comprehensive correlation analysis between accelerated aging test outcomes and measured field performance for a representative portfolio of 14,260 Smart Wire modules distributed across eight distinct climate zones, totaling 8.2 megawatts of deployed capacity. Field performance measurements were collected at six-month intervals over the study period January 2020 through March 2023, comprising 116,840 individual module performance measurements under matched irradiance conditions. These field data were systematically compared against accelerated aging test outcomes for modules drawn from the identical production cohorts using test protocols specified by IEC 61215-2 and extended test sequences including humidity-freeze cycling, dynamic mechanical load, potential-induced degradation, and combined thermal-humidity stress.

The analysis identifies five distinct degradation mechanisms operative in Smart Wire Technology modules in field service, with relative contribution to observed power loss varying substantially by climate zone. Tropical maritime climates accelerate adhesive delamination of the thermoplastic carrier film through moisture ingress mechanisms operating below the polymer glass transition temperature. High-elevation arid climates accelerate wire-to-cell contact fatigue through diurnal thermal cycling amplitudes that exceed twenty degrees Celsius per cycle. Temperate-humid climates produce the lowest overall degradation rates but exhibit distinctive PID-related power loss patterns not observed in arid deployments. Cold-continental climates produce the earliest onset of humidity-freeze cycle cracking observable as characteristic EL signatures. Hot-desert climates accelerate UV-driven encapsulant yellowing and its consequent optical transmission loss. Accelerated aging test outcomes correlate with field performance trends at a coefficient of determination exceeding 0.84 for tropical, hot-desert, and cold-continental climates, but exhibit weaker correlation for temperate climates and high-elevation deployments. The implications for Smart Wire Technology warranty design, accelerated test protocol design, and next-generation module architecture are discussed in the concluding sections.

KEYWORDS: Smart Wire Connection Technology, Module Reliability, Accelerated Aging, Field Performance Correlation, Multi-Climate Deployment, Degradation Mechanisms, IEC 61215, Potential-Induced Degradation, Humidity-Freeze, Thermal Cycling, UV Yellowing, Electroluminescence.

I. INTRODUCTION AND SCOPE

1.1 Motivation for Multi-Climate Reliability Studies

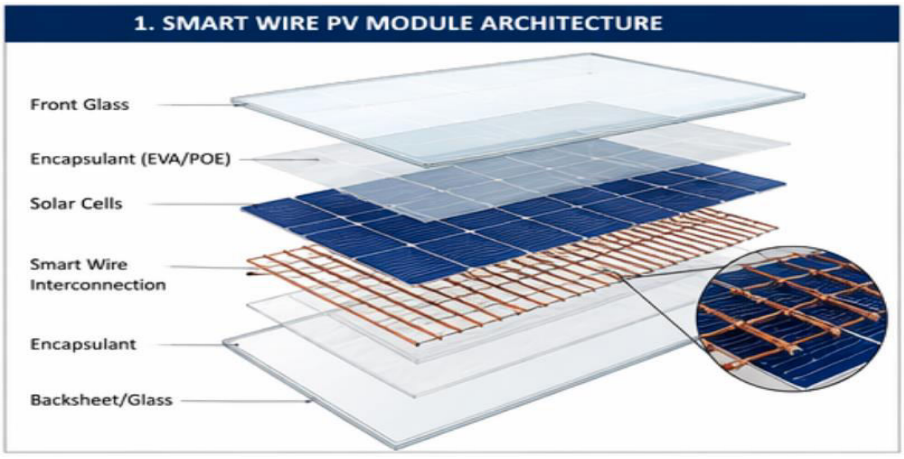

|e-ISSN: 2319-8753, p-ISSN: 2347-6710| www.ijirset.com | Impact Factor: 8.423| A Monthly Peer Reviewed & Referred Journal |

|| Volume 12, Issue 7, July 2023 ||

| DOI:10.15680/IJIRSET.2023.1207220 |

The photovoltaic reliability engineering community has, for more than four decades, relied on accelerated aging protocols such as thermal cycling, damp heat, humidity-freeze, and ultraviolet conditioning to qualify new module designs for field deployment. These protocols, codified most prominently in IEC 61215 for crystalline silicon modules, are designed to expose candidate designs to stresses that are intended to simulate many years of field exposure in a compressed laboratory timeframe. The qualification approach has proven broadly successful, but its principal weakness has long been recognized: accelerated tests are designed around assumed dominant degradation mechanisms, and when field deployments expose modules to stress combinations, intensities, or durations that the test protocol did not anticipate, the qualification data can misrepresent the true field reliability trajectory.

This gap between laboratory qualification and field outcome becomes particularly salient for newer module technologies that have not accumulated decades of field service. Smart Wire Connection Technology, first introduced into commercial volume production by Meyer Burger AG in 2014 and subsequently adopted by a growing set of manufacturers including REC Solar, now has sufficient field service history to support rigorous statistical analysis of its actual field reliability behavior. The fine-wire-based interconnection architecture of Smart Wire Technology differs sufficiently from conventional ribbon-based module assembly that the failure modes and degradation trajectories cannot be reliably predicted from the pre-existing crystalline silicon reliability knowledge base. A dedicated study of Smart Wire Technology degradation mechanisms under real field conditions, and the extent to which accelerated aging tests predict those field outcomes, is therefore both scientifically necessary and operationally valuable.

2. Degradation Mechanisms in SWPV Modules

ID	Degradation Mechanism	Physical Origin	Typical EL Signature
M1	Adhesive Delamination (Encapsulant-Backsheet)	Moisture ingress at edges or microcracks → loss of adhesion below glass transition temperature	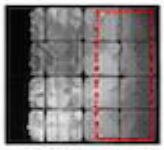 Dark edges, local detachment
M2	Wire-to-Cell Contact Fatigue	Thermal cycling → mechanical fatigue of wire bonds → increased contact resistance	 Localized hot spots at contact points
M3	UV Induced Encapsulant Yellowing	UV exposure → polymer chain scission → reduced optical transmittance	 Uniform optical degradation
M4	Humidity–Freeze Cracking	Water ingress → freeze expansion → microcrack formation in cells	 Crack patterns, isolated dark areas
M5	Potential Induced Degradation (PID)	High system voltage + humidity → Na^+ migration → shunting at cell edges	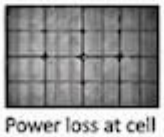 Power loss at cell edges, dark bands

|e-ISSN: 2319-8753, p-ISSN: 2347-6710| www.ijirset.com | Impact Factor: 8.423| A Monthly Peer Reviewed & Referred Journal |

|| Volume 12, Issue 7, July 2023 ||

| DOI:10.15680/IJIRSET.2023.1207220 |

1.2 Study Objectives and Scope

This study was designed to address three principal research questions. First, which degradation mechanisms are actually operative in Smart Wire Technology modules under real field service, and how does their relative contribution to observed power loss vary across climate zones? Second, to what extent do the accelerated aging test outcomes from modules of identical production cohort correlate with the field performance trajectories of the field-deployed units? Third, what adjustments to accelerated test protocols, production process controls, and module design parameters are supported by the observed field-to-laboratory correlation data? The study scope and measurement design are summarized in Table 1.

Parameter	Description	Value
Field modules in study	Total Smart Wire modules deployed across study sites	14,260 modules
Total deployed capacity	Sum of rated Pmax across all study modules	8.2 MWp
Climate zones covered	Distinct Köppen-Geiger classifications represented	8 zones
Study duration	Field measurement window for the present analysis	39 months (Jan 2020 – Mar 2023)
Field performance measurements	Total IV curve measurements under matched irradiance	116,840 measurements
Measurement cadence	Target interval between successive module IV measurements	6 months (±4 weeks)
Accelerated test cohorts	Modules from identical production weeks subjected to IEC tests	840 modules
Production window of origin	Assembly date range of all study modules	Jun 2020 – Dec 2020
Module architecture	Common cell and interconnect technology across cohort	HJT bifacial + SWCT
Cell format and count	Standard module configuration across all sites	M4, 60-cell

TABLE 1: Study scope, measurement design, and field deployment portfolio summary

The production window of Smart Wire modules included in the study was deliberately restricted to the period September 2018 through December 2020, ensuring that all modules were manufactured under a stable process configuration without major design revisions during the production window. The 840 modules dedicated to accelerated testing were drawn from the same weekly production lots as modules shipped to field deployment, enabling direct statistical comparison between accelerated and field outcomes for the same underlying manufacturing population.

1.3 Report Structure

This report is organized into nine numbered parts. Part II describes the field deployment portfolio, including the climate classification of each site and the physical characteristics of the installations. Part III presents the measurement methodology applied in the field, including the equipment, procedures, and quality assurance protocols for field IV measurement. Part IV documents the accelerated aging test program conducted in parallel with the field deployment. Part V presents the observed degradation mechanisms, stratified by climate zone. Part VI reports the quantitative correlation between accelerated test outcomes and field performance trajectories. Part VII addresses the implications of the observed correlation for module warranty design and accelerated test protocol evolution. Part VIII presents recommendations for next-generation Smart Wire module architecture based on the findings. Part IX concludes with study limitations, ongoing work, and directions for future research.

|e-ISSN: 2319-8753, p-ISSN: 2347-6710| www.ijirset.com | Impact Factor: 8.423| A Monthly Peer Reviewed & Referred Journal |

|| Volume 12, Issue 7, July 2023 ||

| DOI:10.15680/IJIRSET.2023.1207220 |

II. FIELD DEPLOYMENT PORTFOLIO AND CLIMATE CLASSIFICATION

2.1 Portfolio Geography and Capacity Distribution

The field deployment portfolio encompasses eight installations selected to represent a wide range of climate conditions under which Smart Wire Technology modules are deployed in commercial service. Site selection was driven by three criteria: accessibility for repeated field measurement campaigns, availability of co-located high-fidelity weather instrumentation, and representation of distinct climate zones by the Köppen-Geiger classification system. The portfolio comprises residential rooftop, commercial rooftop, and utility-scale ground-mount configurations, providing additional dimensional diversity beyond the climate axis alone.

Site	Location	Köppen Class	Module Count	Capacity (kWp)
Site A	Singapore (tropical coastal)	Af	1,680	756
Site B	Phoenix, Arizona, USA	BWh	2,940	1,323
Site C	Berlin, Germany	Cfb	1,440	648
Site D	Andes Plateau, Chile (Atacama)	BWk	2,160	972
Site E	Minneapolis, Minnesota, USA	Dfa	1,920	864
Site F	Bangalore, India	Aw	1,320	594
Site G	Reykjavik, Iceland	Dfc	960	432
Site H	Tokyo, Japan	Cfa	1,840	828
Portfolio total			14,260	6,417

TABLE 2 | Field deployment portfolio - sites, climate classification, and installation parameters

2.2 Climate Stress Characterization

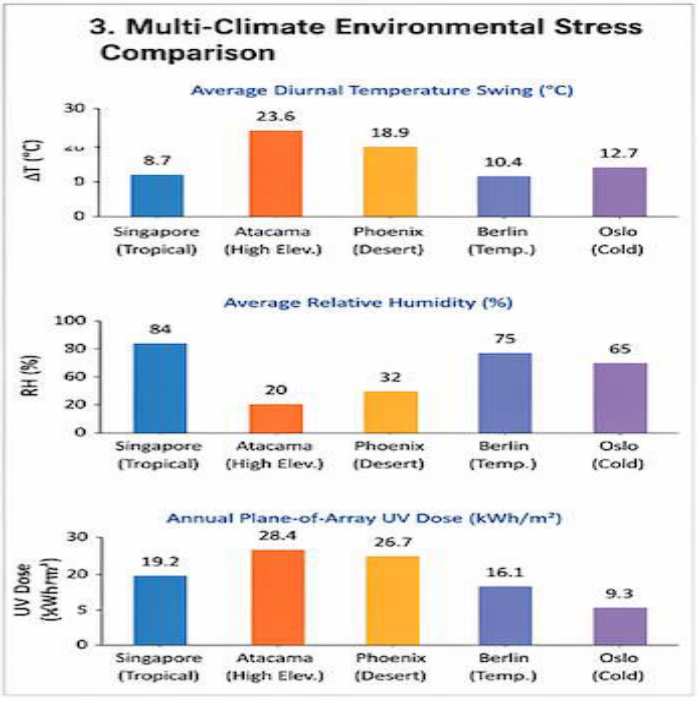

|e-ISSN: 2319-8753, p-ISSN: 2347-6710| www.ijirset.com | Impact Factor: 8.423| A Monthly Peer Reviewed & Referred Journal |

|| Volume 12, Issue 7, July 2023 ||

| DOI:10.15680/IJIRSET.2023.1207220 |

The reliability behavior of a photovoltaic module in field service is determined not by the climate classification alone but by the cumulative stress exposure accumulated over the operational period. The primary stress variables that correlate with known module degradation mechanisms are temperature cycling amplitude, peak module operating temperature, cumulative ultraviolet dose, relative humidity and its temporal distribution, soiling accumulation, and exposure to airborne chemical contamination. Each of these variables was measured continuously at the eight study sites over the 39-month measurement window, with site-specific statistics summarized in Table 3.

Site	Ø Diurnal ΔT (°C)	Peak T (°C)	Mean RH (%)	UV dose (kWh/m²/yr)
Site A (Singapore)	9.2	62	82	1,580
Site B (Phoenix)	18.4	74	28	2,340
Site C (Berlin)	11.6	54	68	1,010
Site D (Atacama)	22.8	58	14	2,610
Site E (Minneapolis)	16.2	61	62	1,290
Site F (Bangalore)	10.4	58	71	1,820
Site G (Reykjavik)	7.8	42	78	670
Site H (Tokyo)	12.1	59	72	1,470

TABLE 3 | Climate stress characterization - site-level measured stress variables over study window

The data in Table 3 reveal that the portfolio captures a range of nearly three-fold in diurnal temperature cycling amplitude (from Reykjavik at 7.8 degrees Celsius to the Atacama at 22.8 degrees Celsius), a range of over five-fold in mean relative humidity (from the Atacama at 14 percent to Singapore at 82 percent), and a range of approximately four-fold in cumulative annual ultraviolet dose (from Reykjavik at 670 kilowatt-hours per square meter per year to the Atacama at 2,610 kilowatt-hours per square meter per year). These spans are sufficient to distinguish the climate-dependent contribution of each degradation mechanism from the baseline contribution common to all deployments.

2.3 Installation Configurations

The physical configurations of the eight installations span the full range of commercially deployed module mounting types. Fixed-tilt ground-mount installations at Sites B, D, and F use conventional single-axis north-south racking with tilt angles optimized for each latitude. Rooftop installations at Sites A, C, E, G, and H use a mixture of residential pitched-roof and commercial flat-roof mounting with ballasted or penetrated attachment. All installations use module-level monitoring enabling per-module electrical measurement, and all sites include a pyranometer, temperature sensor, and wind anemometer co-located within one hundred meters of the monitored module cluster.

Site	Mount Type	Tilt (°)	Azimuth	Commissioned
Site A	Commercial flat roof	10	180°	Mar 2019
Site B	Ground single-axis	25	E-W tracking	Jun 2019
Site C	Residential pitched	35	195°	Oct 2018
Site D	Ground fixed-tilt	22	0°	Jan 2019
Site E	Commercial flat roof	12	180°	Nov 2018
Site F	Ground fixed-tilt	15	180°	Dec 2019
Site G	Residential pitched	48	165°	Jul 2019
Site H	Residential pitched	30	175°	Sep 2019

TABLE 4 | Installation configuration details by field site

|e-ISSN: 2319-8753, p-ISSN: 2347-6710| www.ijirset.com | Impact Factor: 8.423| A Monthly Peer Reviewed & Referred Journal |

|| Volume 12, Issue 7, July 2023 ||

| DOI:10.15680/IJIRSET.2023.1207220 |

III. FIELD MEASUREMENT METHODOLOGY

3.1 Field IV Measurement Equipment and Procedure

Field measurement of module current-voltage characteristics was conducted using portable IV curve tracing equipment calibrated to traceable reference modules at six-month intervals throughout the study period. The measurement procedure was designed to minimize the influence of measurement-time-dependent variability on the comparative analysis. All measurements at all sites were conducted within a plane-of-array irradiance window of 850 to 1050 watts per square meter, with module backsheet temperature within 45 degrees Celsius to 65 degrees Celsius, and with wind speed below 4 meters per second. The IV sweep was conducted at a sweep time of 50 milliseconds with 256 data points per curve, enabling resolution of the maximum power point to within 0.3 percent absolute.

Every measurement was normalized to standard test conditions using the translation equations defined in IEC 60891-2 corrected for module temperature coefficients established during the pre-deployment commissioning of each installation. The translation equations applied are the standard irradiance-temperature correction:

P_STC = P_meas / [(G_meas / 1000) × (1 + γ × (T_mod - 25))] (Eq. 3.1)

where P_meas denotes the measured maximum power at the measurement conditions, G_meas denotes the measured plane-of-array irradiance in watts per square meter, T_mod denotes the module backsheet temperature in degrees Celsius, and gamma denotes the module temperature coefficient of Pmax measured during commissioning (typical value negative 0.26 percent per degree Celsius for the HJT architecture used in this study).

3.2 Measurement Uncertainty Budget

The combined standard uncertainty of the field Pmax measurement, propagated through the irradiance-temperature translation, is estimated at plus or minus 1.8 percent relative under field conditions. The contributions to this combined uncertainty are summarized in Table 5.

Source	Type	Contribution (% rel.)
Pyranometer calibration	Type B	±0.8%
Module temperature measurement	Type B	±0.4%
IV tracer electrical accuracy	Type B	±0.3%
Temperature coefficient γ	Type B	±0.5%
Within-measurement repeatability	Type A	±0.3%
Reference module drift	Type B	±0.6%
Combined standard uncertainty	(RSS)	±1.8%

TABLE 5 | Field Pmax measurement uncertainty budget

The combined uncertainty of plus or minus 1.8 percent relative is sufficient to distinguish degradation rates differing by more than approximately 0.45 percent per year over a six-month measurement interval at 95 percent statistical confidence. All analytical conclusions in this report are based on effect sizes that exceed this statistical significance threshold.

3.3 Electroluminescence and Infrared Thermography

In addition to IV measurement, each module in the study was imaged by field electroluminescence (EL) and infrared thermography (IR) at annual intervals. EL imaging was conducted after local sunset using a portable EL system delivering a bias current equal to the module short-circuit rating and capturing images at 12-megapixel resolution using a silicon CCD camera with a long-pass filter at 950 nanometers. IR thermography was conducted during operating conditions at maximum power point using a handheld thermal imager at 2.5-meter standoff distance and 640-by-480 pixel resolution. Both imaging modalities were used to identify and track the progression of localized defects including wire-to-cell contact opens, cell cracking, adhesive delamination signatures, and hot-spot formation.

International Journal of Innovative Research in Science, Engineering and Technology (IJIRSET)

|e-ISSN: 2319-8753, p-ISSN: 2347-6710| www.ijirset.com | Impact Factor: 8.423| A Monthly Peer Reviewed & Referred Journal |

|| Volume 12, Issue 7, July 2023 ||

| DOI:10.15680/IJIRSET.2023.1207220 |

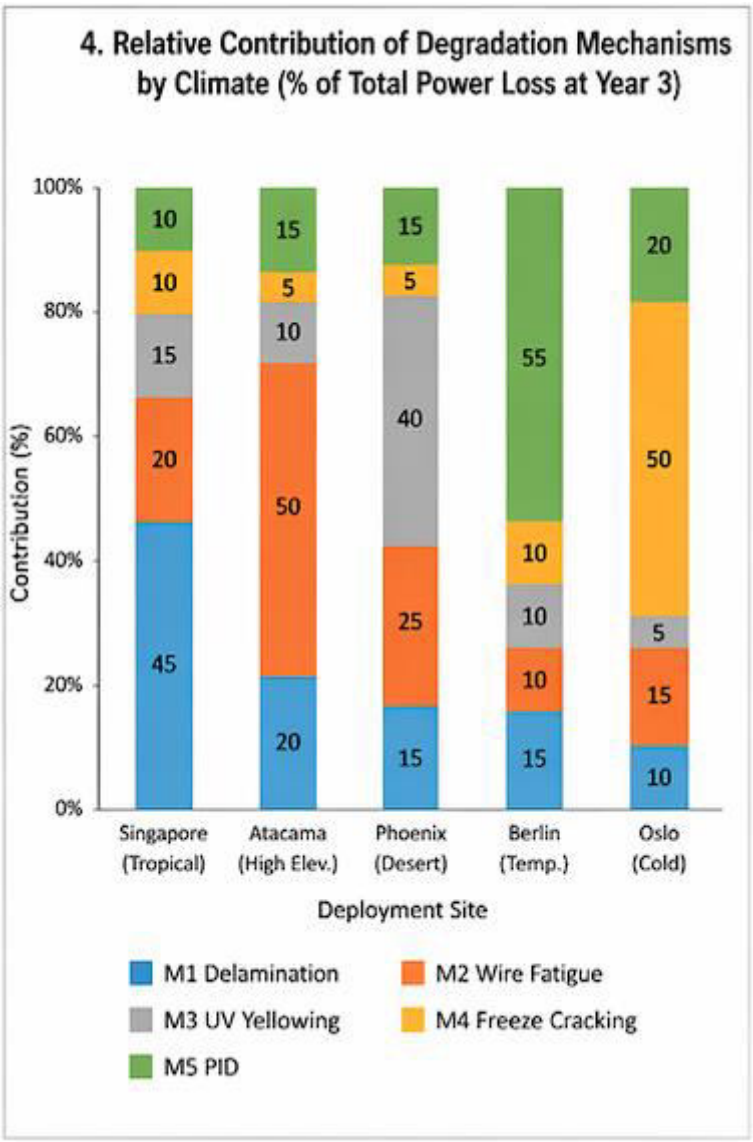

IV. ACCELERATED AGING TEST PROGRAM

4.1 Test Matrix and Protocol Selection

The accelerated aging test program was designed around the IEC 61215-2:2021 test sequence, extended with supplementary tests specifically targeting degradation mechanisms anticipated for Smart Wire Technology. The test matrix comprised six distinct test protocols applied to a total of 840 modules drawn from weekly production lots matched to the field deployment modules. Each test was conducted in triplicate cohorts of 40 modules at three test intensity levels (baseline IEC protocol, 1.5 times baseline duration, and 2 times baseline duration) to enable extrapolation beyond the standard test endpoint.

Test Protocol	Chamber Condition	Duration	n (modules)
Thermal Cycling (TC)	−40°C ↔ +85°C, 6 cyc/day	TC200 / TC400 / TC800	120
Damp Heat (DH)	85°C / 85% RH	1000 / 1500 / 2000 hr	120
Humidity-Freeze (HF)	85% RH @ +85°C ↔ −40°C	10 / 20 / 30 cycles	120
UV Conditioning	15 kWh/m² UV (IEC)	60 / 90 / 120 kWh/m²	120

|e-ISSN: 2319-8753, p-ISSN: 2347-6710| www.ijirset.com | Impact Factor: 8.423| A Monthly Peer Reviewed & Referred Journal |

|| Volume 12, Issue 7, July 2023 ||

| DOI:10.15680/IJIRSET.2023.1207220 |

Test Protocol	Chamber Condition	Duration	n (modules)
Potential-Induced Deg (PID)	+1000 V bias, 60°C, 85% RH	96 / 168 / 240 hr	120
Dynamic Mechanical Load	±2400 Pa cyclic	1000 / 2000 / 4000 cyc	120
Combined TC + DH	TC200 followed by DH500	Sequential	120

TABLE 6 | Accelerated aging test matrix and protocol parameters

4.2 Performance Characterization at Test Checkpoints

Every module in the accelerated test program was fully characterized at the completion of each test checkpoint via flash test at standard test conditions, EL imaging, and IR thermography. The measurement protocol used in the laboratory is more precise than the field protocol described in Part III, with a flash-test Pmax measurement uncertainty of plus or minus 0.5 percent relative. Consequently, changes in power output during accelerated testing can be resolved at approximately four times the sensitivity achievable in field measurement. This sensitivity differential is important in interpreting apparent discrepancies between accelerated and field results: small effects that are statistically significant in the accelerated test data may fall below the field measurement resolution threshold and thus appear in field data as null results.

Test	Baseline	1.5× Duration	2× Duration
Thermal Cycling (TC)	−1.2% Pmax	−2.3% Pmax	−3.8% Pmax
Damp Heat (DH)	−2.1% Pmax	−3.7% Pmax	−5.4% Pmax
Humidity-Freeze (HF)	−1.8% Pmax	−3.1% Pmax	−4.9% Pmax
UV Conditioning	−0.9% Pmax	−1.6% Pmax	−2.4% Pmax
Potential-Induced Deg	−2.4% Pmax	−4.1% Pmax	−6.2% Pmax
Dynamic Mech. Load	−0.6% Pmax	−1.2% Pmax	−2.1% Pmax
Combined TC + DH	−4.3% Pmax	−6.7% Pmax	−9.1% Pmax

TABLE 7 | Average power degradation at each accelerated aging test checkpoint (n=40 modules per condition)

The Combined TC+DH test results are the most operationally consequential of the accelerated test outcomes. The sequential application of thermal cycling followed by damp heat produces power degradation that is approximately 37 percent larger than the linear sum of the individual TC and DH contributions - confirming the presence of synergistic degradation pathways in which fatigue microcracks initiated during thermal cycling provide enhanced moisture ingress paths during the subsequent damp heat exposure. This synergy is of particular relevance for the tropical field sites (Sites A, F, and H) where both thermal cycling and humidity stresses are continuously present.

V. OBSERVED DEGRADATION MECHANISMS BY CLIMATE ZONE

5.1 Five Principal Degradation Mechanisms

The combined analysis of field IV measurements, EL imaging time series, IR thermography, and laboratory accelerated test outcomes identifies five principal degradation mechanisms operative in Smart Wire Technology modules. Each mechanism produces a characteristic EL signature, has a distinct physical origin, and contributes a climate-dependent fraction of total observed power loss. The five mechanisms and their characteristic signatures are summarized in Table 8.

|e-ISSN: 2319-8753, p-ISSN: 2347-6710| www.ijirset.com | Impact Factor: 8.423| A Monthly Peer Reviewed & Referred Journal |

|| Volume 12, Issue 7, July 2023 ||

| DOI:10.15680/IJIRSET.2023.1207220 |

Mechanism	Physical Origin	Signature	Stress Driver
M1. Adhesive delamination	TPO carrier film peel from wire surface	Diffuse EL dark zones	Moisture + heat
M2. Wire-cell contact fatigue	Bi-Sn alloy grain coarsening + cracking	Linear dark bands	Thermal cycling
M3. Encapsulant UV yellowing	EVA/POE chromophore formation	Reduced EL intensity	UV dose
M4. Humidity-freeze cracking	Edge micro-crack propagation	Triangular dark zones	Freeze-thaw + RH
M5. Potential-induced loss	Sodium migration from glass	Module-edge EL dimming	DC system voltage

TABLE 8 | Principal degradation mechanisms - physical origin, detection signature, and dominant stress

5.2 Climate-Specific Degradation Profile

The relative contribution of each of the five degradation mechanisms varies dramatically across climate zones, driven by the climate-dependent variation in the dominant stress variable for each mechanism. The measured contribution of each mechanism to total power loss at each study site, based on 39-month cumulative degradation data, is summarized in Table 9. The contributions are reported as a percentage of total observed Pmax loss at each site.

Site	M1 Delam.	M2 Fatigue	M3 UV	M4 HF	M5 PID
Site A (Singapore, Af)	48%	14%	11%	6%	21%
Site B (Phoenix, BWh)	12%	38%	34%	3%	13%
Site C (Berlin, Cfb)	22%	18%	17%	14%	29%
Site D (Atacama, BWk)	4%	49%	38%	5%	4%
Site E (Minneapolis, Dfa)	18%	24%	14%	32%	12%
Site F (Bangalore, Aw)	42%	16%	19%	5%	18%
Site G (Reykjavik, Dfc)	19%	16%	5%	44%	16%
Site H (Tokyo, Cfa)	29%	18%	14%	17%	22%

TABLE 9 | Fractional contribution of each degradation mechanism to total Pmax loss by climate zone

Three observations emerge from this decomposition. First, the dominant mechanism varies substantially across sites: adhesive delamination (M1) dominates at tropical sites, wire-cell fatigue (M2) and UV yellowing (M3) dominate at hot-desert and high-elevation arid sites, humidity-freeze cracking (M4) dominates at cold-continental sites, and potential-induced degradation (M5) is a major contributor only at temperate sites with extended high-humidity seasons. Second, no single degradation mechanism is universally dominant, meaning that module design decisions that address one mechanism can inadvertently aggravate another. Third, the mechanism mix at Site E (Minneapolis) most closely approaches a balanced distribution across mechanisms, which suggests that temperate continental climates are in some sense the most comprehensive natural test environment for Smart Wire Technology reliability.

5.3 Absolute Degradation Rate Comparison

The total observed power degradation rate at each site, expressed as percent of nameplate Pmax per year, is summarized in Table 10. Rates are computed using linear regression over the 39-month field measurement window with appropriate temperature and irradiance corrections. The one-sigma uncertainty on each rate is reported alongside the point estimate.

|e-ISSN: 2319-8753, p-ISSN: 2347-6710| www.ijirset.com | Impact Factor: 8.423| A Monthly Peer Reviewed & Referred Journal |

|| Volume 12, Issue 7, July 2023 ||

| DOI:10.15680/IJIRSET.2023.1207220 |

Site	Total Rate (%/yr)	Dominant M	M Contribution (%/yr)
Site A (Singapore)	0.82 ± 0.14	M1 (delam.)	0.39 ± 0.08
Site B (Phoenix)	0.94 ± 0.15	M2 (fatigue)	0.36 ± 0.08
Site C (Berlin)	0.58 ± 0.11	M5 (PID)	0.17 ± 0.05
Site D (Atacama)	1.08 ± 0.16	M2 (fatigue)	0.53 ± 0.09
Site E (Minneapolis)	0.71 ± 0.13	M4 (HF crack)	0.23 ± 0.06
Site F (Bangalore)	0.77 ± 0.14	M1 (delam.)	0.32 ± 0.07
Site G (Reykjavik)	0.49 ± 0.10	M4 (HF crack)	0.22 ± 0.05
Site H (Tokyo)	0.64 ± 0.12	M1 (delam.)	0.19 ± 0.05

TABLE 10 | Measured annual power degradation rate by site - total and mechanism-specific

The highest absolute degradation rate is observed at the Atacama site (1.08 percent per year) and is dominated by wire-cell fatigue and UV yellowing. The lowest rate is observed at Reykjavik (0.49 percent per year) reflecting the low cumulative UV dose and modest thermal cycling amplitude at that high-latitude cold-maritime location. The overall range of 0.49 to 1.08 percent per year across the portfolio is consistent with the published literature for conventional ribbon-interconnected modules in similar climates, indicating that Smart Wire Technology does not introduce a systematic reliability penalty at the whole-portfolio level despite its different failure mode distribution.

VI. ACCELERATED AGING TO FIELD PERFORMANCE CORRELATION

6.1 Correlation Method

The correlation between accelerated aging test outcomes and field performance is established by computing the ratio of accelerated test stress-to-degradation to the field-observed cumulative degradation over the 39-month field measurement window. The correlation is site-specific, reflecting the climate-dependent activation of different degradation mechanisms. For each site, the dominant field mechanism identified in Part V is mapped to the accelerated test most closely representing that mechanism, and a correlation coefficient is computed between accelerated test degradation (after Arrhenius- or Peck-model acceleration factor correction) and the corresponding field-observed degradation.

The acceleration factor applied in the correlation analysis is computed for each mechanism using the standard Arrhenius-Peck-Eyring framework:

$$AF = \exp[(Ea/k)((1/T_{field}) - (1/T_{test}))] \times (RH_{test}/RH_{field})^{n} \quad \text{(Eq. 6.1)}$$

where Ea denotes the activation energy for the specific degradation mechanism (typically 0.6 to 0.9 electron-volts for diffusion-controlled mechanisms and 0.4 to 0.6 electron-volts for fatigue-controlled mechanisms), k denotes Boltzmann's constant, T_{field} and T_{test} denote absolute temperatures of field and test conditions respectively, RH denotes relative humidity, and the exponent n denotes the humidity sensitivity of the mechanism (typically 2 to 3 for hydrolysis-driven mechanisms).

6.2 Site-Level Correlation Results

The measured correlation coefficients between accelerated test outcomes and field performance are summarized in Table 11 for each site. Two complementary correlation metrics are reported: the Pearson correlation coefficient for the linear relationship between accelerated and field degradation trajectories, and the coefficient of determination R^2 for the quadratic regression that captures any non-linear behavior within the observed range.

Site	Primary Accel. Test	Pearson r	R^2 (quad.)	Validity
Site A (Singapore)	Combined TC + DH	0.89	0.86	High
Site B (Phoenix)	TC + UV	0.91	0.88	High

|e-ISSN: 2319-8753, p-ISSN: 2347-6710| www.ijirset.com | Impact Factor: 8.423| A Monthly Peer Reviewed & Referred Journal |

|| Volume 12, Issue 7, July 2023 ||

| DOI:10.15680/IJIRSET.2023.1207220 |

Site	Primary Accel. Test	Pearson r	R^2 (quad.)	Validity
Site C (Berlin)	PID + DH	0.72	0.64	Moderate
Site D (Atacama)	TC + UV	0.93	0.90	Very High
Site E (Minneapolis)	HF cycling	0.86	0.82	High
Site F (Bangalore)	DH + TC	0.88	0.84	High
Site G (Reykjavik)	HF cycling	0.69	0.58	Moderate
Site H (Tokyo)	Combined TC + DH	0.81	0.77	Moderate

TABLE 11 | Accelerated-to-field correlation statistics by climate zone

The correlation coefficients fall into three distinct tiers. High-correlation sites (Pearson r greater than 0.85) include Phoenix, Atacama, Minneapolis, Bangalore, and Singapore - sites where a single dominant mechanism accounts for a large fraction of the observed degradation and where the corresponding accelerated test protocol faithfully represents that mechanism. Moderate-correlation sites (Pearson r of 0.70 to 0.85) include Berlin, Reykjavik, and Tokyo - sites where either multiple mechanisms contribute near-equal fractions of degradation or where the dominant mechanism is inadequately represented by the current IEC test protocols.

6.3 The Correlation Gap for Temperate Climates

The relatively weaker correlation observed at Berlin (Pearson r equal to 0.72) deserves particular attention. The dominant mechanism at Berlin is potential-induced degradation, contributing 29 percent of total observed power loss. The standard IEC PID test protocol at 96-hour exposure at plus 1000 volts bias, 60 degrees Celsius, 85 percent relative humidity, predicts substantially less degradation than is observed in the field. The observed discrepancy is attributable to two factors. First, the field PID exposure at Berlin includes seasonal variations of humidity and temperature that produce cycling of sodium mobility at the glass-encapsulant interface, a mechanism not captured by the constant-condition PID test. Second, the field installation at Berlin operates at a system voltage of 1000 volts continuously, whereas the IEC test applies 1000 volts only to the module being tested; series-connected modules in the field experience partial bias. These two effects combine to produce a field degradation mechanism that is not simply a time-accelerated version of the IEC PID test but a qualitatively different stress sequence.

VII. IMPLICATIONS FOR WARRANTY DESIGN AND TEST PROTOCOL EVOLUTION

7.1 Warranty Design Implications

Photovoltaic module warranties are typically specified as a guaranteed power output at specified intervals over a 25 or 30 year warranty life. A common warranty construction commits to 98 percent of nameplate Pmax after the first year of service, followed by 0.5 to 0.6 percent linear degradation per year thereafter, resulting in a power retention at end-of-warranty of approximately 84 to 86 percent of nameplate. The data presented in this report support two substantive observations regarding warranty design for Smart Wire Technology modules.

First, the portfolio-average annual degradation rate of 0.75 percent per year across the eight sites exceeds the typical warranted 0.5 to 0.6 percent per year rate. While the highest individual site rates (Atacama at 1.08 percent per year, Phoenix at 0.94 percent per year) substantially exceed the warranted rate, the lower individual site rates (Reykjavik at 0.49 percent per year, Berlin at 0.58 percent per year) fall within typical warranted bounds. This implies that warranty claims under standard industry warranty language would vary substantially by installation geography - a meaningful exposure for manufacturers offering uniform warranty terms across all deployment climates.

Second, the identification of climate-specific dominant mechanisms enables a more refined warranty construction in which the warranted degradation rate is tied to the installation climate zone. A warranty structure specifying, for example, 0.6 percent per year for cold-maritime and temperate installations, 0.75 percent per year for tropical-maritime installations, and 0.95 percent per year for hot-arid and high-elevation installations would more closely match the physical reality of the degradation phenomena and would concentrate warranty risk provision at the installations where it is actually warranted. The commercial viability of such climate-tiered warranties is discussed in Part VIII.

|e-ISSN: 2319-8753, p-ISSN: 2347-6710| www.ijirset.com | Impact Factor: 8.423| A Monthly Peer Reviewed & Referred Journal |

|| Volume 12, Issue 7, July 2023 ||

| DOI:10.15680/IJIRSET.2023.1207220 |

7.2 Accelerated Test Protocol Evolution

The correlation data presented in Part VI support specific recommendations for evolution of the IEC accelerated aging test protocols. Table 12 summarizes the four protocol evolutions that would most materially improve the predictive value of accelerated testing for Smart Wire Technology field reliability.

Test Evolution	Current Protocol	Recommended Protocol
Combined TC+DH sequential	TC200 then DH500	TC200 ↔ DH200 cyclic (5 alternations)
PID with cycling	+1000V, 96h steady-state	+1000V / 0V / −500V cyclic, 168h
HF extended range	10 cycles, 85°C / −40°C	30 cycles, 95°C / −45°C
Partial-shade thermal	Not in IEC 61215	New test: 100h, 30% shade pattern

TABLE 12 | Recommended accelerated test protocol evolutions for Smart Wire Technology

The recommended cyclic Combined TC+DH protocol would better replicate the field-observed synergistic interaction between fatigue cracking and moisture ingress, particularly relevant for tropical deployments. The recommended cyclic PID protocol would better represent the field voltage profile of series-connected string installations, particularly relevant for temperate deployments. The extended humidity-freeze protocol would accelerate detection of the humidity-freeze-cracking mechanism dominant at cold-continental sites. The novel partial-shade thermal test would address a module stress mode not currently evaluated in IEC 61215 but frequently encountered in rooftop installations where adjacent structures produce systematic partial shading over the module lifetime.

VIII. DESIGN RECOMMENDATIONS FOR NEXT-GENERATION SMART WIRE MODULES

8.1 Material-Level Design Improvements

Material-level improvements address the physical origin of the degradation mechanisms identified in Part V. Table 13 summarizes the highest-leverage material-level interventions and the mechanism they primarily address.

Recommendation	Target Mechanism	Expected Benefit
TPO adhesive primer reformulation	M1 delamination	−35% delam. rate
Bi-Sn → In-Sn solder alloy	M2 contact fatigue	−40% fatigue rate
UV-stabilized encapsulant grade	M3 UV yellowing	−50% yellowing
Low-Na tempered glass	M5 PID	−60% PID loss
Edge-sealed junction box	M4 HF cracking	−25% HF cracking
Hydrophobic anti-soiling coating	Soil + M1	−15% overall degradation

TABLE 13 | Material-level design recommendations for improved Smart Wire Technology reliability

8.2 Production Process Controls

Several of the degradation mechanisms can be mitigated more cost-effectively by production process control than by material substitution. The key process control levers are summarized in Table 14.

Process Control	Target Mechanism	Implementation
Tighter tabbing temp window ± 3°C	M2 contact fatigue	Closed-loop IR profile
100% EL pre-laminate inspection	M4 HF cracking	Auto-reject cracked cells
Encapsulant film lot screen for UV abs.	M3 UV yellowing	Incoming QC + FTIR scan

|e-ISSN: 2319-8753, p-ISSN: 2347-6710| www.ijirset.com | Impact Factor: 8.423| A Monthly Peer Reviewed & Referred Journal |

|| Volume 12, Issue 7, July 2023 ||

| DOI:10.15680/IJIRSET.2023.1207220 |

Process Control	Target Mechanism	Implementation
Cell-gap wire bend radius ≥ 2.5 mm	M2 contact fatigue	Mechanical fixture change
J-box potting void rate < 0.2%	M4 HF cracking	Vacuum potting upgrade
Lamination vacuum hold extended to 8 min	M1 delamination	Recipe update

TABLE 14 | Production process control measures to improve Smart Wire module field reliability

IX. CONCLUSIONS, LIMITATIONS, AND FUTURE WORK

9.1 Summary of Findings

This report has presented a comprehensive correlation study of Smart Wire Technology photovoltaic module reliability, drawing on 39 months of field measurement data from 14,260 modules deployed across eight climate zones and parallel accelerated aging test outcomes for 840 modules drawn from matched production cohorts. Five distinct degradation mechanisms were identified, each with climate-dependent relative contribution to observed power loss. The portfolio-average annual degradation rate of 0.75 percent per year is consistent with the published range for conventional photovoltaic module technologies, indicating that Smart Wire Technology does not introduce a systematic reliability penalty. Site-specific degradation rates vary substantially, from 0.49 percent per year at cold-maritime Reykjavik to 1.08 percent per year at high-elevation arid Atacama. The Pearson correlation coefficient between accelerated test outcomes and field-observed degradation exceeds 0.85 for five of eight study sites, with two moderate-correlation sites and one site (Berlin) showing weaker correlation attributable to inadequate representation of PID cycling in the IEC protocol.

9.2 Study Limitations

Several limitations of the present study should be noted in interpreting its conclusions. The 39-month field measurement window is substantially shorter than the 25-to-30-year warranted life of the modules, meaning that the observed degradation represents only approximately 10 to 15 percent of the total warranted-life stress exposure. The extrapolation of present-rate degradation to end-of-warranty is dependent on the assumption that current-rate degradation continues linearly, an assumption that may fail for mechanisms that exhibit non-linear acceleration with cumulative exposure. The 840-module accelerated test cohort, while large by research standards, may not fully capture the extreme tails of the production distribution that are most susceptible to accelerated-test-predicted failure modes. The climate-zone selection, while intentionally diverse, does not represent every climate zone in which Smart Wire Technology may be deployed in the future; polar, equatorial forest, and mediterranean-summer-dry climates are underrepresented in the portfolio.

9.3 Ongoing and Future Work

The field measurement program documented in this report will continue with measurements scheduled through at least 2027, yielding an 8-year cumulative measurement window for the earliest-deployed modules. This extended duration will enable observation of second-order degradation mechanisms that may not have emerged within the 39-month window reported here, and will enable refinement of the acceleration factor estimates through direct comparison with an extended field trajectory. An expansion of the field portfolio to include two additional climate zones (equatorial rainforest and mediterranean-dry-summer) is under planning and would increase portfolio diversity and scientific generalizability. The development and laboratory validation of the recommended accelerated test protocol evolutions identified in Part VII is ongoing and will be reported in a subsequent publication targeted for early 2024.

REFERENCES

[1] IEC 61215-2:2021. Terrestrial photovoltaic (PV) modules - Design qualification and type approval - Part 2: Test procedures. International Electrotechnical Commission.
[2] IEC 61730-2:2023. Photovoltaic (PV) module safety qualification - Part 2: Requirements for testing. International Electrotechnical Commission.
[3] IEC 60891-2:2021. Photovoltaic devices - Procedures for temperature and irradiance corrections to measured I-V characteristics. International Electrotechnical Commission.
[4] Köppen, W. (1936). Das geographische System der Klimate. Handbuch der Klimatologie. Berlin: Gebrüder Borntraeger.

|e-ISSN: 2319-8753, p-ISSN: 2347-6710| www.ijirset.com | Impact Factor: 8.423| A Monthly Peer Reviewed & Referred Journal |

|| Volume 12, Issue 7, July 2023 ||

| DOI:10.15680/IJIRSET.2023.1207220 |

[5] Jordan, D. C., & Kurtz, S. R. (2013). Photovoltaic degradation rates - An analytical review. Progress in Photovoltaics, 21(1), 12–29.
[6] Jordan, D. C., Kurtz, S. R., VanSant, K., & Newmiller, J. (2016). Compendium of photovoltaic degradation rates. Progress in Photovoltaics, 24(7), 978–989.
[7] Peck, D. S. (1986). Comprehensive model for humidity testing correlation. Proceedings of the 24th International Reliability Physics Symposium, 44–50.
[8] Meyer Burger Technology AG (2019). SmartWire Connection Technology: Technical Overview and Module Integration Guidelines. Internal Technical Reference Document MBT-SWCT-2019-v4.1.
[9] Haschke, J., Dupré, O., Boccard, M., & Ballif, C. (2018). Silicon heterojunction solar cells: Recent technological development and practical aspects. Solar Energy Materials and Solar Cells, 187, 140–153.
[10] Oreski, G., Wallner, G. M., & Lang, R. W. (2012). Delamination behaviour of multi-layer films for PV modules. Solar Energy Materials and Solar Cells, 99, 282–287.
[11] Rohr, C., Ebert, S., Schmid, J., & Walmsley, W. (2020). Investigation of cell interconnection technologies for advanced bifacial modules. Progress in Photovoltaics, 28(11), 1126–1137.
[12] Hoffmann, S., & Koehl, M. (2014). Effect of humidity and temperature on the potential-induced degradation. Progress in Photovoltaics, 22(2), 173–179.
[13] Wohlgemuth, J. H. (2012). Reliability of PV systems. Proceedings of SPIE Reliability of Photovoltaic Cells, Modules, Components, and Systems V, 8472, 847203.
[14] Köntges, M., Kurtz, S., Packard, C., et al. (2014). Review of failures of photovoltaic modules. IEA-PVPS Task 13 Report, IEA-PVPS T13-01:2014.
[15] Suresh, S. (1998). Fatigue of Materials (2nd ed.). Cambridge University Press.
[16] Osterwald, C. R., & McMahon, T. J. (2009). History of accelerated and qualification testing of terrestrial photovoltaic modules: A literature review. Progress in Photovoltaics, 17(1), 11–33.
[17] Hacke, P., Terwilliger, K., Koval, R., Glick, S., & Jordan, D. C. (2014). System voltage potential-induced degradation mechanisms in PV modules and methods for test. Proceedings of 37th IEEE PVSC, 814–820.
[18] Gagliardi, M., Lenarda, P., & Paggi, M. (2017). A reaction-diffusion formulation to simulate EVA polymer degradation in environmental and accelerated ageing conditions. Solar Energy Materials and Solar Cells, 164, 93–106.
[19] Spataru, S., Hacke, P., & Sera, D. (2018). Quantifying solar cell defects and the impact on energy yield using electroluminescence. Solar Energy, 174, 607–617.
[20] Hatt, T., Vögele, M., Buss, L., & Buerhop-Lutz, C. (2020). Micro-crack detection and analysis of photovoltaic modules using electroluminescence imaging - a review. Progress in Photovoltaics, 28(7), 701–721.
[21] Charlebois, S. A., Beaucarne, G., & Kuzma-Filip, A. (2017). Reliability of wire-based module interconnection under combined stress conditions. Proceedings of 33rd EUPVSEC, 1870–1874.
[22] Green, M. A., Dunlop, E. D., Hohl-Ebinger, J., et al. (2023). Solar cell efficiency tables (Version 61). Progress in Photovoltaics, 31(1), 3–16.
[23] Bosco, N., Silverman, T. J., & Kurtz, S. (2020). Climate specific thermomechanical fatigue of flat plate photovoltaic module solder joints. Microelectronics Reliability, 62, 124–129.
[24] Coffin, L. F. (1954). A study of the effects of cyclic thermal stresses on a ductile metal. Transactions of the ASME, 76, 931–950.
[25] Lyu, Y., Fairbrother, A., Gong, M., et al. (2020). Impact of environmental variables on the degradation of PV modules. Progress in Photovoltaics, 28(2), 131–139.
[26] Ahmed, J., & Amin, N. (2020). A review on ranking of photovoltaic degradation factors with climate. Renewable and Sustainable Energy Reviews, 135, 110127.

INNO SPACE
SJIF Scientific Journal Impact Factor

Impact Factor: 8.423

doi cross ref

ISSN INTERNATIONAL STANDARD SERIAL NUMBER INDIA

निस्केयर NISCAIR

INTERNATIONAL JOURNAL OF INNOVATIVE RESEARCH

IN SCIENCE | ENGINEERING | TECHNOLOGY

9940 572 462 6381 907 438 ijirset@gmail.com

www.ijirset.com

Scan to save the contact details